CERN-PPE/95-86
14 June, 1995

The DELPHI Silicon Strip Microvertex Detector with Double Sided Readout

V. Chabaud, P. Collins, H. Dijkstra, J. J. Gomez Cadenas, R. Keranen, S. Masciocchi, W. Trischuk, P. Weilhammer
CERN, CH-1211, Geneva 23, Switzerland

Y. Dufour
Collège de France, Lab. de Physique Corpusculaire, IN2P3-CNRS, F-75231 Paris Cedex 05, France

R. Brenner, R. Orava, K. Osterberg, C. Ronnqvist, H. Saarikko [1], J.-P. Saarikko, T. Tuuva, M. Voutilainen
Research Institute for High Energy Physics, SEFT, P.O. Box 9, FIN-00014 Helsinki, Finland

J. Błocki, P. Brückman, J. Godlewski, P. Jałocha, W. Kucewicz, H. Pałka, A. Zalewska
High Energy Physics Laboratory, Institute of Nuclear Physics, Ul. Kawiory 26a, PL-30055 Krakow 30, Poland

B. Bouquet, F. Couchot, B. D'Almagne, F. Fulda-Quenzer, P. Rebecchi
Université de Paris-Sud, Lab. de l'Accélérateur Linéaire, IN2P3-CNRS, Bât. 200, F-91405 Orsay Cedex, France

P. P. Allport, P. S. L. Booth, P. A. Cooke
Department of Physics, Univ. of Liverpool, P.O. Box 147, Liverpool L69 3BX, UK

A. Andreazza, P. Biffi, V. Bonvicini, M. Caccia, C. Meroni, M. Pindo, N. Redaelli, C. Troncon, G. Vegni
Dipartimento di Fisica, Università di Milano and INFN, Via Celoria 16, I-20133 Milano, Italy

J. Cuevas Maestro
Dpto. Fisica, Univ. Oviedo, C/P. Pérez Casas, S/N-33006 Oviedo, Spain

G. J. Barker, J. Bibby, N. Demaria, M. Flinn, P. Pattinson
Dept. of Nuclear Physics, Univ. of Oxford, Keble Road, Oxford OX1 3RH, UK

M. Mazzucato, A. Nomerotski[2], A. Peisert, I. Stavitski
Dipartimento di Fisica, Università di Padova and INFN, Via Marzolo 8, I-35131 Padova, Italy

M. Baubillier, F. Rossel
LPNHE, IN2P3-CNRS, Universités Paris VI et VII, Tour 33 (RdC), 4 place Jussieu, F-75252 Paris Cedex 05, France

M. Gandelman, D. Santos de Souza
Centro Brasileiro de Pesquisas Físicas, rua Xavier Sigaud 150, RJ-22290 Rio de Janeiro, Brazil

R. Apsimon, M. Bates, J. Bizzell, P. D. Dauncey, L. Denton, W. Murray, M. Tyndel
Rutherford Appleton Lab., Chilton, Didcot OX11 OQX, UK

J. Marco, C. Martinez-Rivero
C.E.A.F.M., C.S.I.C. - Univ. Cantabria, Avda. los Castros, S/N-39006 Santander, Spain

M. Karlsson
Fysikum, Stockholm University, Box 6730, S-113 85 Stockholm, Sweden

J. A. Hernando
IFIC, Valencia-CSIC and D.F.A.M.N., U. de Valencia, Avda. Dr. Moliner 50, E-46100 Burjassot (Valencia), Spain

(Submitted to Nuclear Instruments and Methods in Physics Research)

[1] currently at Department of Physics, University of Helsinki, P.O. Box 9, FIN-00014 Helsinki, Finland.
[2] on leave from the Budker Institute of Nuclear Physics, Novosibirsk, 630090, Russia.

Abstract

The silicon strip Microvertex detector of the DELPHI experiment at the CERN LEP collider has been recently upgraded from two coordinates ($R\phi$ only) to three coordinates readout ($R\phi$ and z). The new Microvertex detector consists of 125952 readout channels, and uses novel techniques to obtain the third coordinate. These include the use of AC coupled double sided silicon detectors with strips orthogonal to each other on opposite sides of the detector wafer. The routing of signals from the z strip to the end of the detector modules is done with a second metal layer on the detector surface, thus keeping the material in the sensitive area to a minimum. Pairs of wafers are daisy chained, with the wafers within each pair flipped with respect to each other in order to minimize the load capacitance on the readout amplifiers. The design of the detector and its various components are described. Results on the performance of the new detector are presented, with special emphasis on alignment, intrinsic precision and impact parameter resolution. The new detector has been taking data since spring of 1994, performing up to design specifications.

1 Introduction

1.1 Physics motivation

High precision silicon strip vertex detectors have become an important tool to improve charged particle track reconstruction and study long lived particle decay vertices in high energy physics experiments. After successful use of silicon strip detectors in fixed target experiments since the beginning of the 1980s for the study of charmed particles, new detectors have been built and successfully operated in experiments at high energy colliders, both e^+e^- and $p\bar{p}$ [1, 2].

DELPHI [3], one of the four large multi-purpose experiments running at the LEP e^+e^- collider at CERN, has operated with a silicon strip Microvertex detector since the start-up of LEP in 1989. It first consisted of two concentric layers of single sided silicon detectors, with AC coupled readout strips, with 50 μm pitch, oriented to provide high precision measurements of charged particle tracks in the plane transverse to the beam [3]. The addition of a third layer became possible in 1991, after the reduction of LEP beam pipe diameter, due to the low beam backgrounds. A detailed description of the first DELPHI silicon strip vertex detector can be found in ref. [1]. The performance of this detector can be summarized by the single hit precision of about 8 μm, averaged over all track incidence angles and cluster sizes and including alignment uncertainties, and by the hit efficiency of 98%. This resulted in an impact parameter uncertainty well described by $\sqrt{(69/p_t)^2 + 24^2}$ μm, (p_t in GeV/c) determined from hadronic Z^0 decays.

The use of information from the previous Microvertex detector has led to a large improvement in charged particle impact parameter and momentum resolution and has resulted in improved physics capabilities, in particular in the detection and study of long lived particles. These include the precision measurements of the τ lepton [4] and b flavoured hadron lifetimes [5], and improvements in b quark identification using lifetime tags. The use of microvertex detectors has also enabled detailed studies of B hadron masses and decay modes via the reconstruction of their final states, including newly discovered particles such as the B_s^0 [6, 7].

A further improvement in lifetime measurements and in the efficiency for identification and reconstruction of heavy quark final states, to be achieved by means of high precision three dimensional tracking, was the motivation for the construction of the new Microvertex.

This detector was installed in the spring of 1994, and is reported on in this paper. Figure 1 shows a hadronic Z^0 decay. The $R\phi$ view is similar to that obtained from the previous detector, but now the event topology in the Rz plane is also precisely reconstructed.

A further upgrade, which will increase the solid angle coverage, is planned for 1996 [8]. This will improve the sensitivity of the experiment, particularly for Higgs searches at LEP2.

1.2 Design considerations of the new Microvertex detector

The upgrade of the Microvertex detector was designed to provide three coordinate readout, satisfying the following requirements:

- The precision in the transverse plane should not be degraded with respect to the previous detector.
- The amount of material crossed by the tracks should not be increased, in order to maintain good impact parameter resolution for low momentum tracks.
- The precision along the z direction should be comparable to that in $R\phi$, in order to improve the vertex reconstruction precision. The significance of the impact parameter d/σ_d of a track from a secondary vertex is shown in fig. 2 as a function of the angle α between the impact distance $\bar{d}$

[3] R, ϕ, z define a cylindrical coordinate system. $+z$ is coincident with the electron beam and R, ϕ define the transverse plane.

and the z strip direction. The lever arms of $R\phi$ and z hits are assumed to be the same and the effect of multiple scattering has been ignored. The gain in significance of the three dimensional impact parameter falls off rapidly unless the z resolution is close to the $R\phi$ resolution.

- The solid angle coverage was to be maintained and possibly enlarged.

These conditions were met by using double sided silicon detectors, with orthogonally oriented readout strips on opposite faces of the detector wafer. In order to maintain the same material thickness, DELPHI developed double sided detectors with a second metal layer on the ohmic surface, making it possible to read-out the signal from both sides at the same end of the detector.

In this paper, the new features of the detector are described, while we refer to [1] for the parts that remain unchanged. Details of the new double sided silicon detectors are given in section 2, together with their acceptance tests. The geometrical configuration is presented in section 3, the front end electronics and data acquisition system in section 4. The offline reconstruction of data is given in section 5, while the alignment procedure is described in section 6 and the performance within DELPHI is discussed in section 7.

2 Detectors

2.1 Separation of n strips

An active direction of research in silicon detectors is the development of readout on both sides of one piece of silicon, allowing three coordinate measurements for the same amount of material. This is difficult because of an electron accumulation layer at the Si-SiO_2 interface on the ohmic side (hereafter referred to as the n-side) of the detector. This accumulation layer results in interstrip resistances of the order of a few kΩ and the charge is shared over many readout strips.

In order to localize signals on n^+ strips they must be insulated from one another. Several solutions have been proposed to disrupt the electron layer, falling into two categories. One uses blocking p^+ electrodes between the n^+ strips and the other uses field plates over the strips to create a field to repel the electrons. Since the latter was pioneered by DELPHI [9], it will be described in detail. In the case of DELPHI the detector order was split over two companies. One supplier[4] used the field plate technique, while the other supplier[5] preferred blocking p^+ electrodes.

Detectors with integrated coupling capacitors have the additional advantage that the metal readout lines can be used as field plates. A cross section of such a structure is shown in fig. 3. It looks like a cross section of the junction side (hereafter referred to as the p-side), but the metal line is wider, extending outside the diffusion strip. Studies were performed to optimize the width of the metal lines. Field plate voltages which differ from the depletion voltage (the voltage of the n^+ strips) by more than 10 V result in strip separations greater than 100 MΩ, sufficient to collect the charge deposited by particles on separate strips.

As a test of strip separation, a light spot with a diameter of 30 μm is focused on the surface of the detector and moved across the strips in small steps. Pulse heights on the strips around the light spot are recorded and the fraction of charge collected on a given strip is calculated for each light spot position and is plotted as a function of strip number (see fig. 4).

Curves a) and b) are measured on the n-side while the light spot is shining on the p-side. The light is shone on the opposite side of the detector to avoid possible surface effects caused by light directly exciting the readout lines. In this way all the charge collected is deposited in the silicon and drifts through the depleted detector. Curve a) shows the charge sharing when the strip separation is not complete, i.e. when the field plate voltage differs from the n^+ strip voltage by less than 5 V while

[4] SINTEF, Oslo, Norway.
[5] Hamamatsu Photonics K.K., Hamamatsu City, Japan.

curve b) shows the good separation achieved for field plate voltages beyond 15 V. Curve c) shows the corresponding distribution on the p-side where no such strip separation problem exists.

The biasing scheme for normal operation of the double sided detectors with integrated coupling capacitors is as follows. Advantage is taken of the capacitive coupling of the diffusion lines to the readout lines, by setting all the readout lines to near ground so that the readout electronics input can be at or near ground. The choice of applying a positive voltage to the n^+ strips while leaving the p^+ strips at ground has been made, since this is most radiation hard [10]. The readout lines on the n-side, which remain at ground, then create the desired field plate effect.

This biasing scheme has the potential drawback that the coupling oxide has to sustain the full depletion voltage. This has not posed serious problems in practice as will be shown in section 2.5.

2.2 The silicon readout with a double metal layer

Detectors with readout on both sides are ideally used to measure orthogonal coordinates. This normally requires the readout electronics to be mounted along two edges, increasing the material thickness and distributing the heat load throughout the volume of the detector. To overcome these performance limiting problems a process was developed using two layers of metal (each about 1 μm thick) separated from each other by an insulating layer. The first layer capacitively couples to the n^+. Two separate approaches to insulate the second metal layer have been used in the production of the DELPHI detectors, since the two suppliers proposed different techniques:

- a low temperature deposition of oxide over the whole surface including the metal (Hamamatsu);
- an application of a film of Polyimide, with an electric permittivity of 0.3 pF/cm (SINTEF).

In both cases contacts are opened in the insulating layer and the second metal layer is deposited on top making the desired connections between the first metal layer and the orthogonal readout lines. The top lines run parallel to the p^+ diodes on the other side of the silicon. In this way all the signals can be readout at a common edge of the detector where the readout electronics can be mounted.

Since the detectors are not square there are more n^+ strips than p^+ strips in order to have similar resolution on both sides. For this reason the second metal layer is also designed to multiplex the n^+ strips combining the readout of two or more strips on one line. Information from other tracking detectors of DELPHI is used to resolve the ambiguities.

The construction of double sided double metal layer detectors with integrated coupling capacitors and polysilicon resistors requires 12 to 15 masks compared with the 5 masks necessary to produce a single sided detector. Figure 3 shows a perspective view of the structure. Figure 5 shows the top view of one corner of the n-side of a detector. The outermost wide line is the bias line, providing the depletion voltage to the strips through the polysilicon resistors. The second wide line surrounding the strips is the guard ring. It serves to channel unwanted leakage currents, typically found at the edge of detectors due to initial lattice imperfections exposed in the cutting of the silicon, away from the active volume of the detector. The horizontal diffusion lines (n^+ strips), covered on most of their length by field plates, end by forming a small square pad. This pad is a contact to a metal line, running across the guard ring to connect the bias resistors with the big square pads. The contacts between the bias resistors and the bias line are also represented by squares along the bias line. The coupling capacitors are integrated on the detector by separating the field plates from the n^+ strips with a layer of silicon dioxide. The n^+ strips are visible on the figure since they are longer than the black metal lines and they end in rectangular rings surrounding the contact holes. This ring also serves to interrupt the accumulation layer between the n^+ strips and the guard ring. All these structures are on the first layer since they are peripheral to the active area of the detecor. Figure 6 shows the pattern of contacts between the two metal layers on one of the detectors.

One of the critical parameters determining the detector performance is the load capacitance, which determines the signal to noise ratio that can be expected for the detection of charged particles and

ultimately limits the position resolution. In most cases the load capacitance is dominated by that of one strip to adjacent strips. With integrated coupling capacitors, the measured capacitance is a combination of the inter strip capacitance and the direct capacitance between the diffusion lines and the metal lines. This is further complicated by the introduction of the second metal readout layer. The detectors have 4-5 μm Polyimide (SINTEF) and SiO_2 (Hamamatsu) of insulation, to minimize the contribution of inter-metal capacitance.

The field plate separation of the n-side strips and the double metallization being novel designs a test was performed to check the radiation hardness of these detectors. A detector was irradiated by a Sr^{90} source up to 400 Gy and an extra 170 Gy was added with a 10 MeV e^- beam. Immediately after irradiation the noise went up by 20% and then gradually decreased returning to its original level after one week. No change in dark current was observed. The strip separation on the n-side was checked with a laser and no change was observed. Hence no effect was observed after 570 Gy, to be compared to a maximum accumulated dose of 9 Gy in 1994.

2.3 Acceptance Tests

The detectors received from SINTEF had to be tested strip by strip since they were not fully checked before being delivered. The ones received from Hamamatsu arrived fully tested and only a few of these were selected for spot checks to verify that they matched the required specifications. The criteria for accepting detectors is listed below.

- The number of imperfections found by visual inspection should affect less than 1% of the channels.
- The leakage current measured on the bias line should be less than 10 μA.
- The poly-silicon resistors should have resistances higher than 5 MΩ.

  These limits for the biasing resistors and leakage current ensured that they did not add more than 500 electrons noise when the detectors were connected to readout chips.
- The coupling capacitance should be between 10-20 pF/cm to ensure good charge collection and no capacitive losses to neighbouring strips.
- The number of n-side punch-throughs (pinholes in the insulation layer of the integrated coupling capacitors) should be less than 1% at 20 V above the depletion voltage. For the n-side this is critical since one pinhole, occurring after installation, results in the loss of about 50 neighbouring strips.

Among the detectors received from SINTEF 70% were selected. Most of those rejected had insufficiently high polysilicon resistance for use in DELPHI. Among the ones received from Hamamatsu 99% were accepted.

2.4 Electrical tests

In order to search for problems (such as high noise regions caused by defects in the crystal structure of the silicon) for which the parameters used in section 2.3 are insensitive, it was necessary to test every module electrically during production. The noise performance of each module was measured and a laser was focussed on the detector surface to a spot size of ~ 50 μm and scanned across the surface in such a way that the response of each p and each n^+ strip could be measured. Detectors with dead (low laser response) and insensitive (high noise) regions could be identified and the performance of each module quantified. It was found to be necessary to reject a small number of detectors (10% of SINTEF detector) during module production.

Table 1: Number of pinholes created during long term test of the detectors at a bias voltage of 90 V

	Closer	Outer
Number of channels	44544	64000
Testing time	Number of pinholes	Number of pinholes
1-2 days	19	9
3-4 days	2	3
5-60 days	2	1

In addition, the response of a sample of modules to 60 keV photons from a Am^{241} radioactive source was measured. It was verified that there were no charge collection problems in the detectors, and that the modules would give adequate signal to noise performance.

2.5 Long term punch-through tests of the double sided detectors

The AC coupling of the strips to the readout electronics allows the electronics to remain at ground potential. For double-sided detectors this results in a voltage difference across this capacitor on one of the sides equal to the bias voltage. In case of breakdown this results in large current going into the front end electronics from the neighbouring strips. The noise on these strips increases dramatically. The average number of affected strips is typically 50. This can be cured by removing the bond between the detector and the electronics chip. This does not result in a loss of efficiency since the charge deposited on an unconnected strip is collected by the neighbouring strips. However, it causes a degradation of precision.

After production all modules were over biased at 90 V to provoke the creation of pinholes in weak places. Currently 192 double-sided detectors are running in DELPHI at the bias voltage of 65 V. Table2.5 gives the number of pinholes created in 100 Outer layer and 116 Closer layer silicon detectors tested at 90 V bias voltage as a function of time. The table does not include the pinholes already present at detector delivery. During the whole 1994 data taking only one pinhole has occurred in the Outer layer, which reduced the total efficiency by 0.04 %.

3 Mechanical Design

The mechanical structure of the new Microvertex detector is similar to the previous detector. It consists of three concentric layers of silicon microstrip detectors at average radii of 6.3, 9.0 and 10.9 cm within the central region of the DELPHI detector surrounding the beam pipe. The two layers at average radii 6.3 and 10.9 cm, called the Closer and the Outer, consist of double sided silicon strip detectors, while the Inner layer, at 9.0 cm, consists of single sided detectors. The Outer layer covers the angular region between 44^0 and 136^0. The Inner layer spans from 37^0 to 143^0, the Closer has been extended to cover the region between 25^0 and 155^0 in anticipation of a further upgrade [8]. A schematic view of the detector is presented in fig.7. As for the previous Microvertex detector, each layer consists of 24 modules, each of them built with 4 silicon detectors. Detector pairs are wire bonded in series and read out at both ends of full module.

3.1 The flipped module design

Traditionally the two detectors forming a half module are joined together by daisy-chaining p-side readout lines to p-side ones and n-side to n-side. However, since the readout lines of both sides of

the detectors are at the same potential there is no fundamental problem in joining the n-side of one detector to the p-side of the other detector. This so-called flipped module (fig. 8) has the advantage that the noise on the two sides of the detector is equalized. A single 6 cm long p-side gives a signal to noise ratio (S/N) of 35, while the corresponding n-side gives 22. The S/N for daisy chaining two p-sides is 24, for two n-sides it is 14 and a n-side joined to a p-side gives 18. Hence flipping one of the two detectors improves the signal to noise for n-side measurements, at the expense of higher noise for p-side measurements. S/N performance on the n-side is at a premium because for tracks crossing the silicon at large angles the charge is shared on more strips. Flipping one detector has the added benefit that the signal polarity tags which detector produced a signal. This increases the information provided by the detector at the expense of having to treat signals of both polarities. Figure 8 shows the resulting signal polarities from the different detectors.

3.2 The Double Sided Closer Layer

A Closer layer half module consists of two silicon detectors 7.9 cm and 6.1 cm long by 2.1 cm wide, manufactured by SINTEF, daisy chained using the flipped module design.

The specifications for these detectors are described in table 3.2 and the layout for a module is shown in fig. 9. The p-side includes 768 diodes (25 μm pitch) every second of which is read out. The diodes on the p-side are laid out parallel to the long side of the detector and used to measure the track $R\phi$ coordinate. On the n-side, the first detector has 1152 n^+ diode strips. These are arranged in two compartments of 384 strips of 49.5 μm pitch and a third compartment with 384 strips of 99 μm pitch (fig. 6). This last compartment covers a polar angle between 59^0 and 39^0 in DELPHI. The second detector has only one compartment of 384 strips on the n-side (150 μm pitch). The different strip pitches are chosen to optimize the resolution. The track crossing angle decreases going towards the end of the modules and the deposited charge spreads across over a wider region. Since the position information only really comes from the cluster edges, if the cluster is spread across too many strips, the resolution is degraded due to the constant detector electronics noise level; therefore a coarser pitch becomes advantageous. For both detectors, all strips are read out using the second metal layer. Each readout line on the second metal layer is connected to one strip from each compartment. For the longer detector, there are three contacts between each readout line and first metal line and only one for the shorter one. Thus 384 readout lines run along the n-side, parallel to the diodes on the p-side.

In order to separate the depletion voltages on each detector, a bias line is added to the edge of the 6.1 cm detector, to route the 70 V needed to deplete the 7.9 cm detector. This line consists of a ceramic bar glued along the detector with gold film on the side.

The half module is assembled by gluing the hybrid to a detector with 1.15 mm of overlap and then gluing two detectors together with 1.6 mm overlap. Half modules are glued together to form a full module giving a total length of sensitive silicon of 27.3 cm. A 270 μm thick Ω shaped kevlar beam is glued along the module to achieve a sufficient stiffness. A deviation of 2.6 μm/g of pressure has been measured. Such stiffness is needed mainly to minimize the systematic error of the mechanical survey, described below. Taking into account the overlap between the detectors of each module and the overlap between modules, the average radiation length for this layer is 0.5 %, at 90^0.

3.3 The Double Sided Outer Layer

An Outer layer half module consists of two silicon detectors 5.75 cm long by 3.2 cm wide, manufactured by Hamamatsu. These are joined to make a module 22.68 cm long. There is 1.6 mm between the two silicon detectors. The p-side includes 1280 diodes (25 μm pitch), every second of which is read out through AC-coupled readout lines. These strips run parallel to the long edge of the detector and measure $R\phi$. On the n-side, the detector closest to a polar angle of 90^0 in DELPHI has 1280 strips (42 μm pitch) on the n-side. The second metal readout layer multiplexes them into two compartments to match the 640 readout lines on the p-side. The second detector has 640 strips on the n-side (84

Table 2: Specifications of silicon detectors with double sided readout

	Closer (SINTEF)		Outer (Hamamatsu)	
Thickness(μm)	307		320	
dimensions (cm $\times$ cm)	7.9 $\times$ 2.1; 6.1 $\times$ 2.1		5.75 $\times$ 3.2	
n-type doping	phosphorus		phosphorus	
resistivity (kΩ/cm)	3-6		3-6	
	P side	N side	P side	N side
n^+ strips separation		Field plates		P stops
diffusion strip pitch (μm)	25	49.5, 99, 150	25	42, 84
Readout strip pitch (μm)	50	49.5, 99, 150	50	42, 84
diffusion strip width (μm)	6	8	12	14
Al strip layer 1 width (μm)	8	17	8	8
Al strip layer 2 width (μm)		9		6
Insulator (4-5 μm)		Polyimide		SiO_2
coupling oxide thickness (nm)	$150-250$	$150-250$	$150-250$	$150-250$
coupling capacitance (pF/cm)	10-20	20-50	10	20
polysilicon resistance (MΩ)	4-25	4-25	>10	>20
fraction of pin holes	0.3 %	0.3 %	$< 1\%$	$< 1\%$
multiplexing		3 ; 1		2 ; 1
number of readout channels	384	384	640	640

μm pitch), all of which are read out, with no multiplexing. Here again the tracks cross the silicon at a relatively large angle with respect to the normal and hence a large pitch gives the optimum resolution.

The Outer layer detectors will be re-used as part of '96 upgrade. A different technique was used to stiffen the modules, consisting of edge stiffeners that can be easily removed allowing the extension of the module length. These are ceramic rails 3.5 mm wide, 0.6 mm thick and 6 cm long. A ceramic piece with a groove 350 μm width and 350 μm deep is glued to the edge of the 320 μm thick detectors. A series of such rails is used to stiffen first the half modules and later the pair of half modules that make up a full module. This stiffening minimizes systematic errors during the mechanical survey as in the Closer layer. A deviation of 1.6 μm/g was measured. The average thickness of the Outer layer is 0.5% of a radiation length at 90^0, taking into account the overlaps.

3.4 The Single Sided Inner layer

The Inner layer is built with single sided silicon detectors, with integrated coupling capacitors and biasing resistors. Every second of the 24 modules consists of detectors with a sensitive width of 2.56 cm (512 channels), while the others have a sensitive width of 3.2 cm (640 channels). The length of all detectors is 5.9 cm giving a full module length of 23.6 cm. These silicon detectors have been reused from the Inner and Outer layers of the previous Microvertex detector [1] respectively. This configuration results in a large ($\sim$ 20 %) overlap between neighbouring modules, useful in the alignment of the detector, while creating a layer with an average thickness of 0.5% of a radiation length at 90^0, taking into account the overlaps.

3.5 Half-shells

The detector modules described in the previous sections are assembled into two half-shells. Twelve detector modules per layer are mounted on aluminium end-rings. The modules themselves hold the two end-rings together. Cooling water flows through channels inside the end-rings to remove 180 W from the readout electronics.

4 Front end electronics and data acquisition

The single sided detectors of the Inner Layer are wire bonded to MX3 read out chips, already used in the previous Microvertex detector and described in [11].

For the double sided detectors, the read out lines on both sides of the detectors are wire bonded to MX6 readout chips which are mounted on both sides of a beryllium oxide readout hybrid.

The single multiplexed analogue output from the 10 or 6 MX6 chips (required to read out 640 + 640 channels or 384 + 384 respectively, for Outer or Closer layers) or from the 4 or 5 MX3 chips (Inner Layer) is amplified by repeater electronics and sent to the counting room, where it is digitized by one of 48 SIROCCO units. This design is the same as used in the previous Microvertex detector.

4.1 MX6 chip

The Microplex (MX6) readout chip is a 128 input channel amplifier [12]. The MX6 is a new version of the Microplex family originally designed at the Rutherford Appleton Laboratory [11], in which the charge sensitive preamplifier has been modified to improve the signal to noise ratio. It has been produced in a 3 μm CMOS technology. The output channels are daisy chained, and read out at 2.5 MHz. For a peaking time of 1.5 μs, the measured noise performance of this chip is $[340 + 20 \times C]$ ENC, where C is the capacitance at the input in pF.

The equivalent series noise resistance is 380 Ω and the gain is 0.5 μV/electron with a channel to channel stability of better than 2%. The power consumption is 0.2 W/chip for the 128 channels. A functional diagram of the electronics is given in fig. 10.

To check the radiation hardness some MX6 chips have been exposed to successive 100 Gy doses up to 400 Gy with a γ source ($Cs^{137}, E_\gamma = 662$ keV). It was found that the S/N varies linearly with the dose, reducing the S/N by 8.5% for every 100 Gy of dose. During 1994 modules accumulated between 1 and 9 Gy depending on their position.

4.2 Data acquisition

The data acquisition system has been expanded with respect to the previous Microvertex detector. In order to deal with the increased number of channels (a factor 1.7 larger than previously) the number of SIROCCO Fastbus modules has been increased to 48, corresponding to 96 digital signal processors DSP56001, used for pedestal calculation, noise computation and zero suppression.

The procedure to search for channels with interesting data has been changed in order to treat signals of both polarities, that come from the flipped modules. This implies a further factor two increase in the number of noise hits.

Since tracks are not necessarily perpendicular to the detectors but can cross them at angles as small as 25^0, the cluster search on the n-side has been modified to allow for a variable number of strips per cluster. A cluster is accepted if the signal to noise ratio of one, two or three neighbouring channels is greater than $4\sqrt{n}$, where n is the number of channels. Channels which satisfy this cut (plus a few of their neighbours) are recorded on tape for later analysis. This procedure compresses the 125952 channels into typically 8 kbyte for a hadronic Z^0 event or 4 kbyte for an empty event.

5 Offline Reconstruction

After the clusters have been defined, their positions are calculated in the local coordinate systems of the silicon detectors and then transformed into the DELPHI reference frame. The resulting points are associated to tracks that have been reconstructed in the other tracking detectors of DELPHI.

5.1 Cluster reconstruction

A channel is included in a cluster if its pulse-height (S) to noise (N) ratio is greater than 2.5 on the p-side and 1.4 on the n-side, allowing for the larger spread of the n-side clusters at larger incidence angles and the most probable S/N value. For n-side clusters, the width is compared to the expected one, in order to recover clusters that were split by dead strips or by the Landau fluctuations of the charge deposition. A cluster is accepted only if the sum of the channel S/N ratios is greater than 5.

The position where the particle traversed the silicon is calculated from the charge distribution between the channels. The larger pitch chosen for larger track incidence angles avoids having the charge spread out over too many strips. On the p-side, the impact position is reconstructed by interpolation of the two highest consecutive signals of the cluster and correcting for non linear charge sharing evaluated from

$$\eta = S_{i+1}/(S_i + S_{i+1})$$

Based on studies of beam test data [13], all n-side clusters with incidence angle less than 15° are treated similarly, since the distance traversed by the particles in the detector plane perpendicular to the strips is smaller than the pitch. For larger incidence angles, the traversed distance is sufficiently large that most of the information is contained in the channels at the cluster edges. The position is then the midpoint between the first (head) and the last (tail) channels, corrected with

$$\omega = [\min(S_{\rm head}, \bar{S}) - \min(S_{\rm tail}, \bar{S})]/(2\bar{S})$$

where $\bar{S}$ is the average pulse-height of all channels in between [13]. The minimum of $S_{\rm head/tail}$ and $\bar{S}$ is used to avoid fluctuations due to tails in the Landau distribution.

The distribution of the cluster signal-to-noise ratio (sum over channels) is shown in figure 11 for all three layers. The signal has been multiplied by $\sin\theta$, where θ is the polar angle of the associated track, to account for the longer path (larger signal) of tracks with larger incidence angles. The most probable S/N is 17:1 for both types of hits in the Outer layer, 12:1 for the Inner layer, 13:1 for the Closer layer $R\phi$ hits and 11:1 for the Closer z hits. The difference between $R\phi$ and z for the Closer layer arises because most of the $R\phi$ hits see the noise from the 6 cm long n-side without multiplexing, while most of the z hits are on the 7.9 cm long n-side with three-fold multiplexing.

Since the signal-to-noise ratio is sufficiently good, the charge distribution is mainly determined by the pitch and the incidence angle. As the particles create equal numbers of electrons and holes in the silicon, both sides give the same signal as shown in figure 12.

5.2 Association to tracks

The tracks are first reconstructed without the Microvertex detector, using the points from the Inner Detector (ID), the Time Projection Chamber (TPC) and the Outer Detector (OD). After extrapolation to the Microvertex detector, the tracks are associated to its points, independently for $R\phi$ and z, following the same procedure that was used for the previous detector [1].

This procedure looks for combinations of two Microvertex points in different layers that satisfy certain track-hit residual cuts. A track is forced through each set of two points, keeping the curvature fixed, and additional points are associated in the third layer ($R\phi$) and in the sector overlaps. The cuts depend on the track errors, including the contribution from multiple Coulomb scattering. Although the most common result is three hits in $R\phi$ and two in z, the number of extra hits in the overlaps is large enough to have a significant effect on the average efficiency per layer (section 7.1) and be an important ingredient in the software alignment (section 6). The maximum number of hits per track is six ($R\phi$) or four (z).

Tracks with a single solution are associated first. All solutions with three layers are associated before any with two layers, and all with two layers before any with one layer. There is also an iteration with looser cuts, in order to recover tracks of poorer quality.

The $R\phi$ association runs first and the tracks are refitted. This minimizes the radial uncertainty of z points, thus improving the z residuals.

The multiplexing of the n-side strips does not degrade significantly the pattern recognition, since the possible z positions of each hit are separated by at least 1.9 cm. Possible ambiguities are reduced by the simultaneous association in two layers.

To increase the purity of single $R\phi$ associations, there is a combination of quality cuts together with an upper limit at 1 mm for the track-hit residual cut. The first quality cut requires that the track is seen in the Inner Detector jet chamber and the second one that the signal-to-noise ratio of the Microvertex hit is greater than 8. The third cut requires that the expected number of additional hits is not greater than one, taking into account the geometrical description and a list of known inefficiencies. If the track impact parameter relative to the beam spot is greater than 1 cm, all three quality cuts have to be satisfied. For smaller impact parameters, the purity of single-hit associations is already quite good, as such tracks are more likely to come from inside the Microvertex detector. Thus, any combination of two quality cuts is enough between 1 cm and 1 mm, and only one cut has to be satisfied below 1 mm.

No z association is accepted unless there is at least one $R\phi$ hit on the track. This does not spoil the association efficiency, because a two-layer z association should have at least three $R\phi$ hits and single z associations without $R\phi$ hits would have very low purity.

In addition, the remaining hits are analysed to search for unreconstructed tracks, with an extra constraint from the beam spot or a reconstructed vertex. In hadronic Z^0 decays, on average 1.5 new tracks are found. Some correspond to already reconstructed tracks that were not associated because of interactions in material or distortions due to badly measured points. Some were missed or not properly reconstructed because they were too close to other tracks or to the TPC sector boundaries.

Two new track searches, both of which enhance the role of the Microvertex detector, run in parallel with the standard one. The first one [14] associates Microvertex points to Inner Detector track elements before attaching TPC and OD elements. The second one, developed for the special topology of Z^0 decays into τ leptons, starts with TPC track elements and Microvertex points. In both cases, only the $R\phi$ points are used in the search, while the z points are added later.

6 Alignment

The alignment of the Microvertex detector uses particle tracks from Z^0 decays, taking as a starting point the mechanical survey, from which the relative positions of the modules are known with an accuracy of 25 μm.

After a rough determination of the position of the detector inside the DELPHI reference frame, the alignment is carried out in two stages. First, a purely internal alignment of the Microvertex detector is performed, in which all the modules are allowed to vary their relative positions within the detector. Internal alignment includes a special step intended to remove a possible overall twist of the Microvertex detector. The second stage performs an external alignment of the resulting rigid body with respect to the other tracking detectors of DELPHI. This method has the advantage of restricting the mixing of possible alignment imperfections of the Microvertex and the other detectors to the external alignment stage only, thereby making diagnostics easier.

6.1 Survey

The survey is divided into two different sets of measurements. After assembly, all the modules are individually measured optically to define the strip positions with respect to two reference spheres. Afterwards, when the modules are mounted on the end rings, a full three dimensional survey of the complete half shells is performed before the insertion in DELPHI.

The optical measurement is improved with respect to the procedure described in ref. [1, 15]. A camera[6] with a 250 times magnification mounted on the same 3D measurement station[7] employed for the global survey provides a precision of 2 μm on the focal plane and 15 μm in the coordinate orthogonal to the focal plane. Each module has two high precision machined 4 mm diameter reference spheres positioned on the hybrids. The strip positions on both sides are measured with respect to the reference spheres.

The global half shell survey uses a mechanical probe to measure the position of the reference spheres and of detector planes. The precision of the mechanical survey is 3 μm for the position of the spheres and 23 μm for the detector plane radial position. After folding with the optical measurements, a global survey precision of 25 μm in the strip position is obtained, which is in agreement with results obtained from track residuals before software alignment.

Thanks to the high precision of the optical measurement one can assume in the subsequent software alignment that individual modules are perfectly known rigid bodies, which results in a considerable reduction of the number of degrees of freedom to be dealt with.

6.2 Lorentz drift and barycentric shift

The magnetic field in DELPHI causes the holes and electrons to drift at a small angle relative to the electric field in the detectors. Due to the flipped module design the resulting shift of the reconstructed hit is in an opposite sense in the central and extreme detectors of the Outer or Closer modules. This Lorentz drift can be studied using tracks with hits in all three layers ("3-hit tracks"). The tracks are constrained to pass through the Closer and Outer layer hits and residuals are formed at the Inner layer. Fig. 13 shows the mean $R\phi$ residual as a function of the z coordinate of the track in the Outer layer. Two jumps appear at the transition between central and extreme detectors of Outer layer modules, corresponding to a Lorentz drift of 6 μm. This value is consistent with that obtained using a previous method [1], which can be applied to both the Closer and Outer layers.

During this study it was also found that the barycentres of the distributions of holes and electrons do not correspond exactly to the mid-plane of the detectors. For the holes in the Outer (Closer) layer this new effect can be seen when studying the $R\phi$ residuals in Outer (Closer) layer of hadronic tracks passing through the overlap region of two adjacent sectors ("overlap tracks"). Fig. 14 shows the mean $R\phi$ residual in the Outer layer as a function of the z coordinate of the track in the same layer. The two jumps correspond again to the transition between central and extreme detectors. Using the relative inclination of the two plaquettes (15^0) we deduce a barycentric shift of 10.5 μm. The shift can also be measured in z, using a similar method. The effect is not expected to be the same for holes or electrons, nor for the different layers, and separate corrections are applied.

Note that Lorentz drifts are invisible with overlap tracks since the E-field direction is the same in adjacent detectors. Conversely, the effect of $R\phi$ barycentric shift is suppressed in 3-hit tracks since the majority of the tracks pass through a region where the detector planes are parallel, and hence a radial displacement induces no $R\phi$ shift.

The Lorentz drift in $R\phi$ as well as the $R\phi$ and z barycentric shifts are corrected for before proceeding to the Microvertex detector alignment.

6.3 The software alignment procedure

A detailed account of the alignment procedure can be found in [16].

The procedure uses overlap tracks and 3-hit tracks, defined in the previous section, as well as tracks from Z^0 decays into muon pairs which pass through two opposite sectors ("$\mu\mu$ tracks"). The only information taken from the other tracking detectors is the particle charge and transverse momentum,

[6] Mondo Machine Developments Ltd., Leicester UK.
[7] POLI S.p.A, Varallo Sesia, Italy.

except for $\mu\mu$ tracks which are assigned a momentum equal to the precisely known beam energy. The acollinearity of the beams is also taken into account.

After installation the Microvertex detector position with respect to the other detectors is known with a few mm precision. Using loose criteria for the association of hits to external tracks, the first $\mu\mu$ tracks are used to refine this positioning to better than 100 μm.

In the internal alignment procedure the three layers are treated differently. The Outer layer is treated as "the master layer" and aligned using all possible $R\phi$ and z constraints from overlap tracks. Next the Closer layer modules are aligned individually with respect to the corresponding modules of the Outer layer. Finally the Inner layer modules are aligned individually with respect to the corresponding modules of Outer and Closer layers in the same sector.

For either half shell of the Outer layer, overlap tracks allow the determination of the relative $R\phi$ translation and rotation of all modules, as well as their relative radial displacement and z translation. Still for the Outer layer, tracks at the top and bottom overlaps of the two half shells allow the determination of the three relative translations and the three relative rotations of the two half shells, as well as the determination of a possible relative twist between them. For the Closer layer, the similar $R\phi$ translation and rotation of individual modules, as well as their radial displacement and z translation are determined with respect to the corresponding modules of the Outer layer, using $\mu\mu$ tracks. Once Closer and Outer layers are internally aligned, individual modules of the Inner layer are aligned in $R\phi$ with respect to the corresponding Closer and Outer modules, using constraints from 3-hit tracks.

The alignment procedure involves many elementary steps which are performed iteratively. The $R\phi$ and z constraints from overlap tracks are not used for aligning Closer and Inner layers, but the corresponding residuals are used as independent cross-checks of the quality of the overall alignment.

These steps in the internal alignment do not constrain all geometrical variables. For instance module rotations around their "dip" axes (parallel to the z strips) are difficult to measure precisely and at this stage they are ignored.

Given the lightness of the mechanical structure of the Microvertex detector, small twists may be expected about the z axis. A typical twist might correspond to an $R\phi$ shift of the Closer layer strips of 30 μm at $z = 100$ mm. The method used to measure and remove any overall twist is based on the study of the geometrically signed impact parameter of 3-hit tracks with respect to the beam spot as a function of their polar angle θ. Any dependence on θ reveals a twist. To remove such twists one further iteration between twist suppression and internal alignment of the 3 layers is added.

Finally the rigid body obtained from the previous steps is aligned externally. The alignment constants (three translations and three rotations) are determined using muon pair tracks reconstructed in the other tracking detectors of DELPHI.

6.4 Results

The quality of the alignment is best judged when comparing intrinsic hit precision, measured from residuals which suffer little from misalignments, to hit precision obtained from residuals which include remaining misalignments.

Upper limits for $R\phi$ intrinsic precision are measured from residuals of overlap tracks in Outer layer and residuals in Inner layer of 3-hit tracks (Fig. 15). After putting in the appropriate geometrical factor the $R\phi$ intrinsic precision is found to be better than 7.6 μm. The effective hit precision is measured from residuals of overlap tracks in Closer or Inner layers (which have not been used as constraints in the alignment procedure) (Figs. 15 and 16a). One finds hit precisions of 8.8 μm. The excess of this number over the above limit of 7.6 μm indicates the quality of the alignment. This intrinsic precision is also measured from the $R\phi$ missed distance between two muon tracks (Fig. 16a), from which one also derives an asymptotic impact parameter resolution of 20 μm, well reproducing the result obtained with the previous Microvertex detector.

An upper limit for z intrinsic precision is measured from residuals of overlap tracks in Outer layer (Fig. 17). This figure shows the advantage of changing the n-side readout pitch to match the cluster width. From the distribution in the inset one finds an upper limit to the z intrinsic precision of 9 μm at θ =90°. The precision measured from residuals of overlap tracks in Closer layer are about 20 % worse. It is not clear yet whether this is due to detector effects or to misalignment. Fig. 16b gives the z miss distance between two muon tracks as a function of the polar angle. This distribution reaches a minimum of 48 μm at θ=90^0. When compared to the expectation from the hit precision measured from residuals of overlap tracks in Outer and Closer layers, this figure indicates an alignment quality comparable to the one achieved for $R\phi$. From this figure one also derives an asymptotic impact parameter resolution of 34 μm in the Rz plane, at θ=90°.

7 Performance

7.1 Operational experience

The new Microvertex detector has been working reliably in the DELPHI experiment at LEP since the start of the 1994 data taking period, recording 1.5×10^6 Z^0 decays during its first year of operation. The hardware and software systems performed well, participating in the DELPHI data taking 99 % of the time, while encountering very few problems. Nine half-modules out of 144 showed inefficiencies in $R\phi$. In five cases there were problems with the depletion voltage connection. The others were caused by noisy regions on part of a silicon detector. Most of these problems appeared during the run and hence only affected part of the data taking. The sectors with problems in $R\phi$ also had similar problems in z.

Coupling capacitor pinholes on the n-side, a major operational concern (sec. 2.5), were not a problem. Only one pinhole occurred after 10 days of operation at 65 V. After optimization of the depletion voltage, 60 strips on this detector were inefficient.

In total, these effects introduced an inefficiency of 4.7 % for the Closer, 4.7 % for the Inner and 2.1 % for the Outer layer at the end of the run. However, due to the sector overlaps, the probability of recording at least one hit in a layer was 97.5%, 96.4% and 98.2%, respectively.

7.2 Impact parameter resolution

The impact parameter uncertainty, σ_{IP}, has contributions from three independent sources. There is the purely geometric extrapolation uncertainty, σ_0, due to the point measurement error in the Microvertex detector, the uncertainty due to multiple scattering in the beam pipe and the layers of the Microvertex detector, σ_{MS}, and the uncertainty on the position of the primary vertex, σ_V. Thus, ${\sigma_{IP}}^2 = {\sigma_0}^2 + {\sigma_{MS}}^2 + {\sigma_V}^2$.

For each event, the primary vertex was reconstructed, using an iterative procedure to reject outliers. Only events with good χ^2 probability were retained. To suppress any lifetime contribution, an enriched light quark sample was obtained by selecting events with 10 or more tracks in the main vertex. The impact parameter of each track was evaluated with respect to a vertex reconstructed from the remaining tracks. Both the projections in the $R\phi$ and Rz planes were evaluated. These two impact parameter uncertainties can be parametrized as:

$$ {\sigma_{IP_{R\phi}}}^2 = \left(\frac{\alpha_{MS}}{P\sin^{3/2}\theta}\right)^2 + (\sigma_{0,R\phi})^2 \qquad {\sigma_{IP_Z}}^2 = \left(\frac{\alpha_{MS}}{P\sin^{5/2}\theta}\right)^2 + (\sigma_{0,Rz})^2 $$

where α_{MS} is a multiple scattering coefficient [GeV/c·μm] and P is the track momentum [GeV/c]. In both expressions, the first term is due to the multiple scattering contribution and the second one to the track extrapolation uncertainty. Figure 18 shows the measured error on the impact parameter in the $R\phi$ plane as a function of $P\sin^{3/2}\theta$. The vertex position uncertainty, shown by the bottom

curve, has been subtracted. Parametrizing the impact parameter uncertainty in the same way as for the expected distribution gives ${\sigma_{IP_{R\phi}}}^2 = (\frac{65}{P \sin^{3/2}\theta})^2 + 20^2$ μm^2

The impact parameter resolution in the Rz plane depends strongly on the polar angle of the particle track. There are two effects both contributing to degrade the impact parameter uncertainty for not perpendicular tracks. The first is the varying point precision in z and affects the track extrapolation uncertainty, the latter is the larger path in the material and contributes to increase the multiple scattering uncertainty. The effect of these two contributions is illustrated in fig. 19. The impact parameter resolution (including the vertex uncertainty) for tracks around 1 GeV/c is 90 μm and 203 μm for $80^0 < \theta < 90^0$ and $45^0 < \theta < 55^0$, respectively. For tracks above 8 GeV/c, the corresponding values are 46 μm and 98 μm.

In figure 20, the impact parameter uncertainty is displayed as a function of P for the same angular intervals as before. Here, the vertex reconstruction uncertainty has been subtracted. The asymptotic values are 39 μm and 96 μm, respectively, matching well the result obtained from the dimuon miss distance at the same angles. The multiple scattering coefficient α_{MS} is 71 GeV/c$\cdot\mu$m.

The effect of adding the z information from the new Microvertex detector can be seen in fig. 21, where the impact parameter in the Rz plane is shown both with and without the Microvertex z hits, for nearly perpendicular tracks above 6 GeV/c. (In both cases, the $R\phi$ hits have been used in the track fit.) There is nearly a factor 20 improvement in the Rz impact parameter precision.

8 Conclusions

The DELPHI Microvertex detector has been upgraded from two coordinates to three coordinates readout. It has been operating successfully since the start of the 1994 LEP run.

This detector provides $R\phi$ and z coordinates using newly developed double-sided silicon microstrip detectors, which have the signals from the z strips routed to the end of the detectors by a second metal layer on the detector surface, without any additional material in the active region. The new MX6 chip improved the noise performance. The most probable signal-to-noise ratio for minimum ionizing particles at normal incidence, measured with Z^0 decay tracks, is 17 for both z and $R\phi$ in Outer layer detectors and 11 for z and 13 for $R\phi$ in Closer layer detectors.

The intrinsic resolution is 7.6 μm in $R\phi$ and 9 μm in z (for perpendicular tracks). The impact parameter uncertainty is 20 μm in $R\phi$ and 34 μm in Rz (for perpendicular tracks), as measured from the dimuon miss distance and confirmed by a study of hadronic Z^0 decays.

The performance of the new detector meets the design specifications. The z coordinate provides major improvements in both the precision and overall quality of reconstructed tracks, enhancing the potential of the DELPHI detector in many physics analyses.

Acknowledgements

The detector could only be constructed thanks to the dedicated effort of many technical collaborators in all laboratories participating in the project. We wish to express our appreciation to all of them and in particular to B. Boulter, F. Chignoli, R. Leoni, K. Ratz, A. Rudge.

References

[1] N. Bingefors et al., Nucl. Instr. and Meth. **A328** (1993) 447.

[2] G. Batignani et al. Nucl. Instr. and Meth. **A326** (1993) 183.
P.P. Allport et al. Nucl. Instr. and Meth. **A324** (1993) 34.
P.P. Allport et al. Nucl. Instr. and Meth. **A346** (1994) 476.
S.Tkaczyk et al. Nucl. Instr. and Meth. **A342** (1994) 240.

[3] P. Aarnio et al. (DELPHI Collaboration), Nucl. Instr. and Meth. **A303** (1991) 233.

[4] P. Abreu et al. (DELPHI Collaboration), Phys. Lett. **B267** (1991) 422.
P. Abreu et al. (DELPHI Collaboration), Phys. Lett. **B302** (1993) 356

[5] P. Abreu et al. (DELPHI Collaboration), Z. Phys. **C53** (1992) 567.
P. Abreu et al. (DELPHI Collaboration), Zeit. Phys. **C57** (1993) 181
P. Abreu et al. (DELPHI Collaboration), Phys. Lett. **B311** (1993) 379
P. Abreu et al. (DELPHI Collaboration), Phys. Lett. **B312** (1993) 253
P. Abreu et al. (DELPHI Collaboration), Zeit. Phys. **C61** (1994) 407

[6] P. Abreu et al. (DELPHI Collaboration), Phys. Lett. **B289** (1992) 199.

[7] P. Abreu et al. (DELPHI Collaboration), Phys. Lett. **B324** (1994) 500.

[8] DELPHI Collaboration, Proposal for the upgrade of DELPHI in the Forward Region, DELPHI 92-142, GEN 135.

[9] B. B. Avset et al. A new microstrip detector with double-sided readout, Proceedings of IEEE Nuclear Science Symposium, IEEE trans.nucl.sci.: 37 (1990) 1153-1161.

[10] H. Dijkstra et al., Radiation hardness of Si strip detectors with integrated coupling capacitors, Proceedings of IEEE Nuclear Science Symposium, IEEE trans.nucl.sci.: 36 (1989) 591-592.

[11] P. P. Allport et al., NIM A273 (1988) 630-635.

[12] J. Ardelean et al., NIM A315(1992) 393.

[13] C. Troncon, Measurement of spatial resolution in double sided double metal silicon microstrip detectors, DELPHI 93-21, GEN 141, MVX-3.
H. Dijkstra, J.J. Gomez-Cadenas, J.A. Hernando, C. Troncon, D. Zontar, A study of the resolution of double sided silicon detectors, DELPHI 94-50 TRACK 79.

[14] M. Blume, G. Sciolla, M. Caccia, Study of a combined ID-VD pattern recognition, DELPHI 95-18 PROG 212.

[15] A. Andreazza et al., Nucl. Instr. and Meth. A312 (1992) 431

[16] V. Chabaud et al., The alignment of the DELPHI silicon strip Microvertex Detector with double sided readout, DELPHI note in preparation.

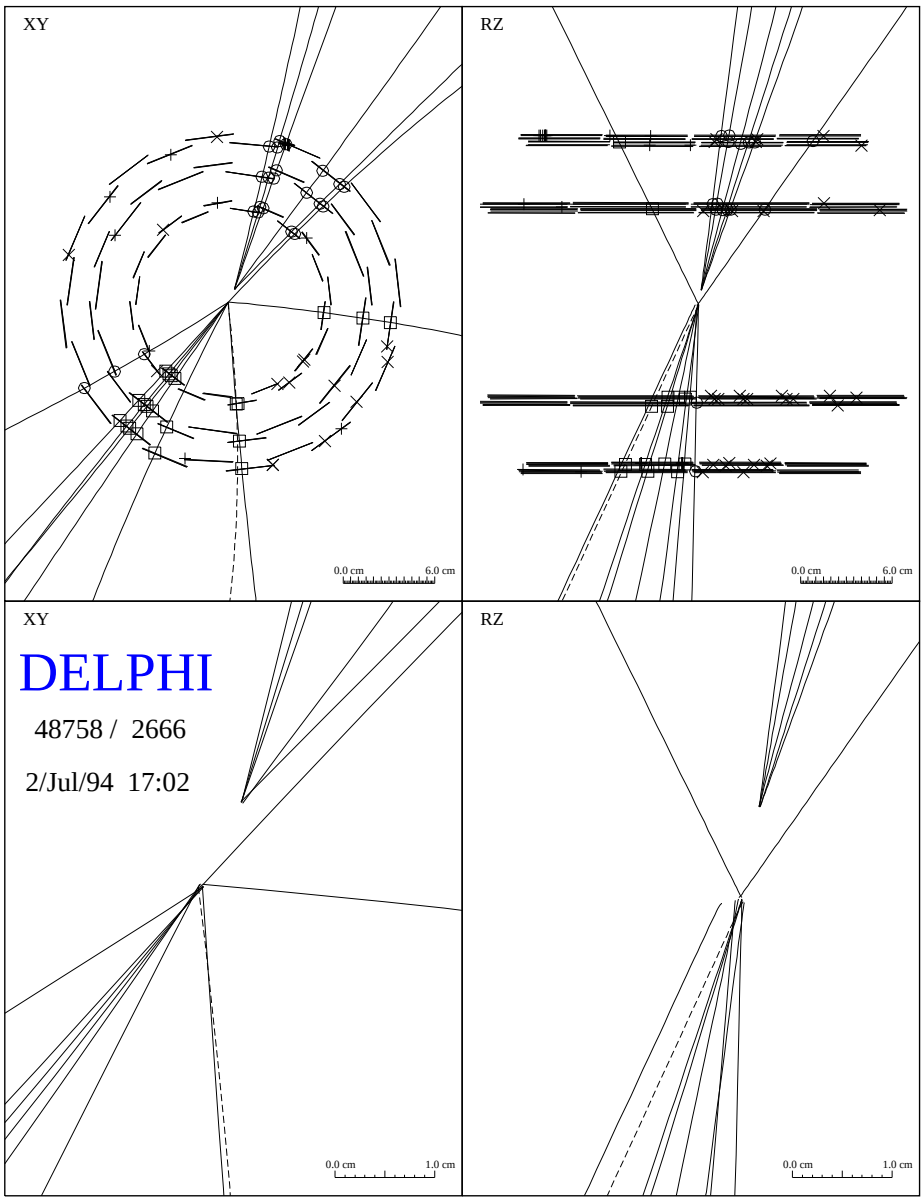

Figure 1: The XY and the Rz projection of one hadronic event from a Z^0 decay observed in the DELPHI Microvertex detector. Circles and squares indicate silicon hits associated to tracks, crosses correspond to unassociated hits. All ambiguous solution are displayed for the unassociated hits. The Rz view is obtained by taking the radial distance to the primary vertex, and signing R according to the hemisphere. Tracks displayed with a dashed line have only one associated hit in that view.

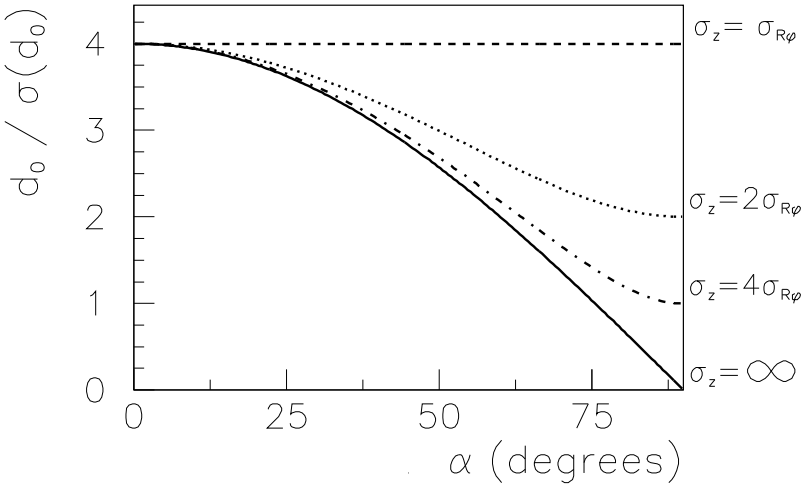

Figure 2: Dependence of the impact parameter significance $d/\sigma(d)$ on the angle α between the direction of the impact parameter distance and the z strip direction. As an example, the significance of a track with an impact parameter $d = 4\sigma_{R\phi}$ is plotted. The solid line follows the $\cos\alpha$ dependence of the xy projected impact parameter d_{xy}, whereas the constant dashed line displays the case of the significance of 3-D impact parameter with equal $R\phi$ and z resolutions. The dotted (dash dotted) lines indicate the significance of 3-D impact parameters from the $R\phi, z$ hit data with z hit precision twice (four times) the $R\phi$ resolution.

Figure 3: Cross sectional view of a complete double-sided double metal detector, showing the p and n implants on the insulating layer/double metal structure on the n-side.

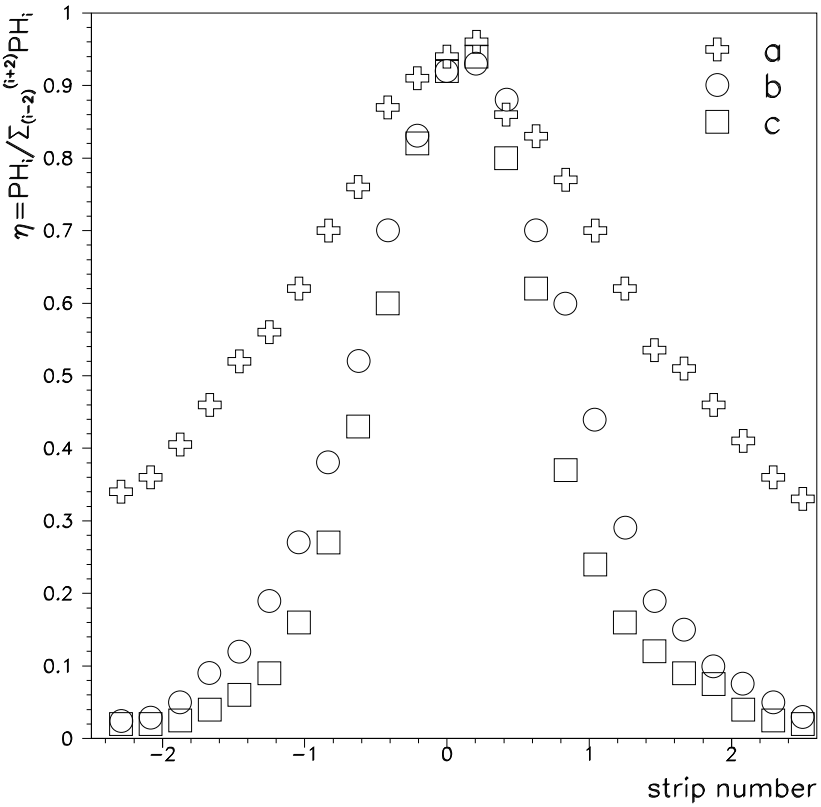

Figure 4: The distribution of charge induced by a 30 μm diameter lightspot for a) a field plate voltage of 5V (no separation), b) a field plate voltage of 15V (strips are separated) and c) the charge separation obtained on the p-side of the detector.

Figure 5: A top view of one corner of a Closer layer detector.

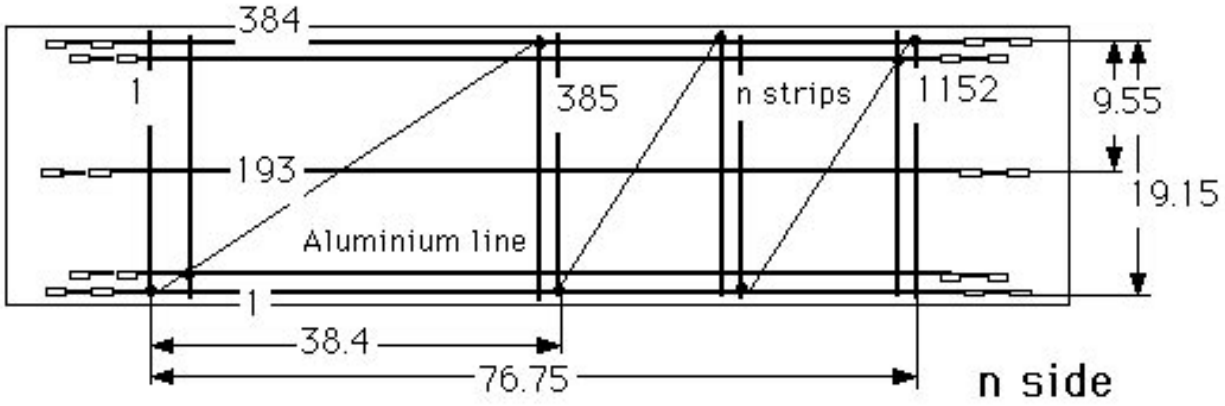

Figure 6: The pattern of contacts between the two metal layers of a Closer layer detector.

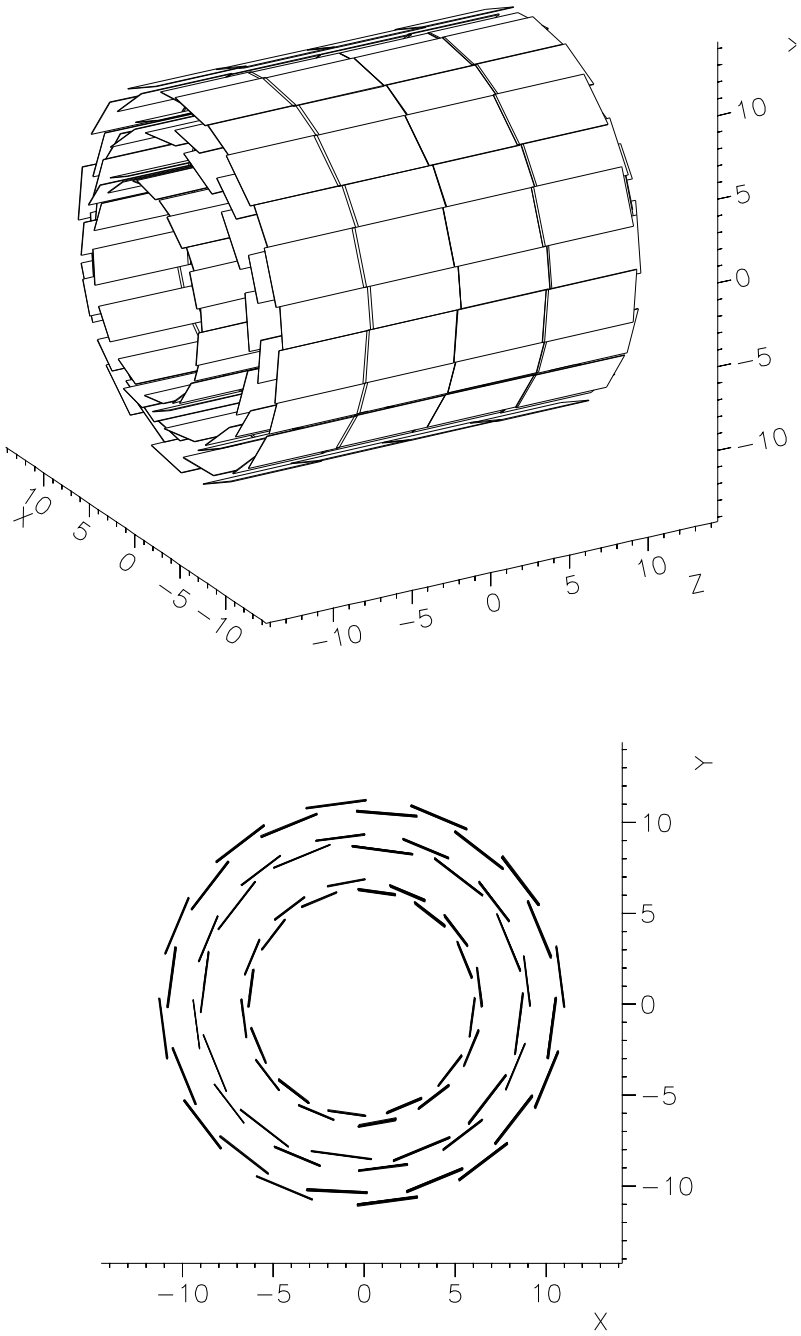

Figure 7: Schematic layout of the new DELPHI Microvertex detector (in cm). a) Perspective view. b) Projection on the plane transverse to the beam.

Figure 8: A schematic drawing of the flipped module concept. Chip 1 will register a negative (positive) signal from track A (B), while chip 2 will register a positive (negative) signal from track A (B). Positive signals correspond to Rϕ coordinates, while negative signals give the z-coordinate of tracks.

Figure 9: A schematic drawing of one Closer module and one Outer module.

Figure 10: Functional diagram of the readout electronics.

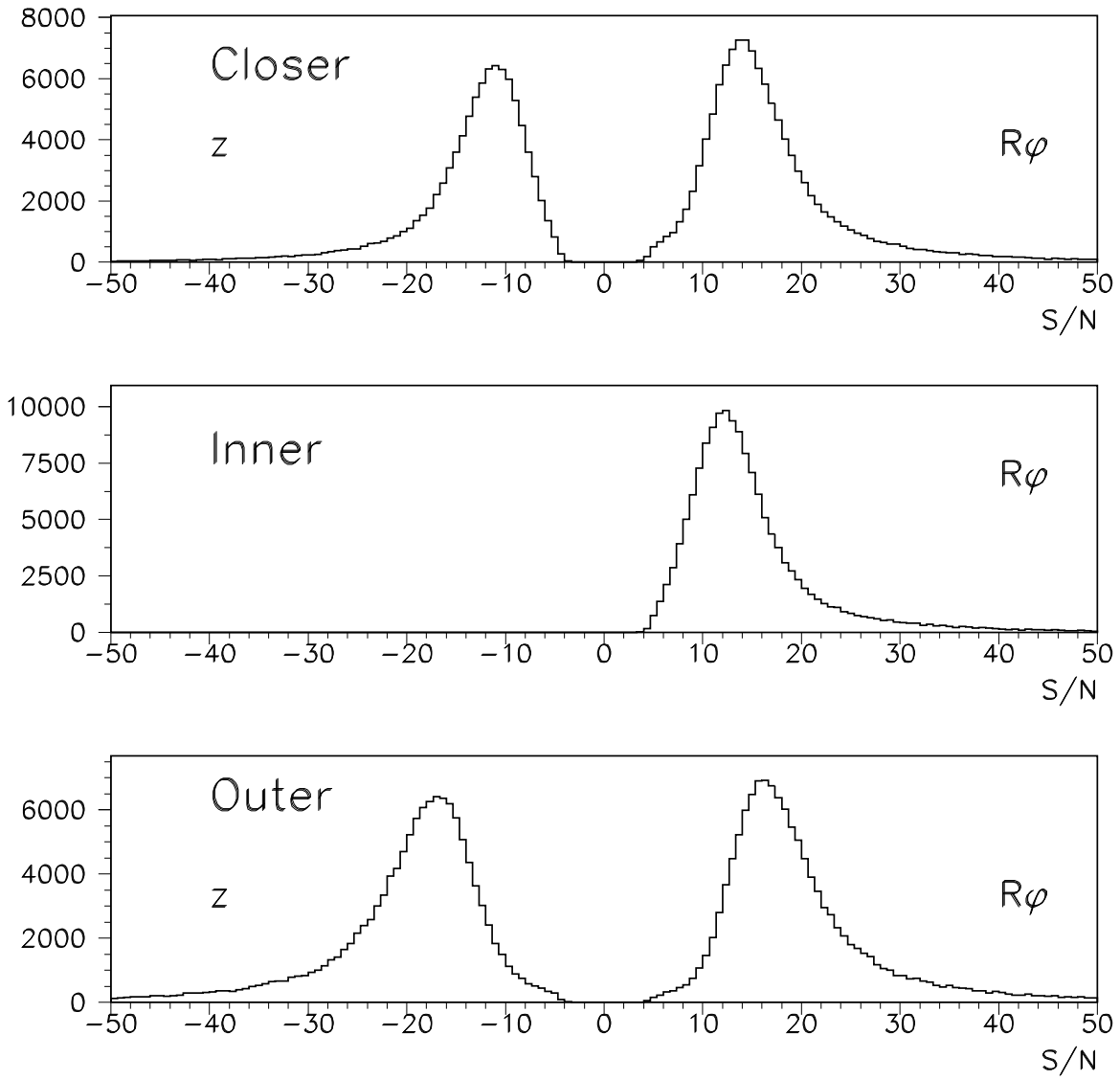

Figure 11: Signal-to-noise ratio, corrected with $\sin\theta$, where θ is the polar angle of the associated track, to account for the varying path lengths of tracks through the silicon.

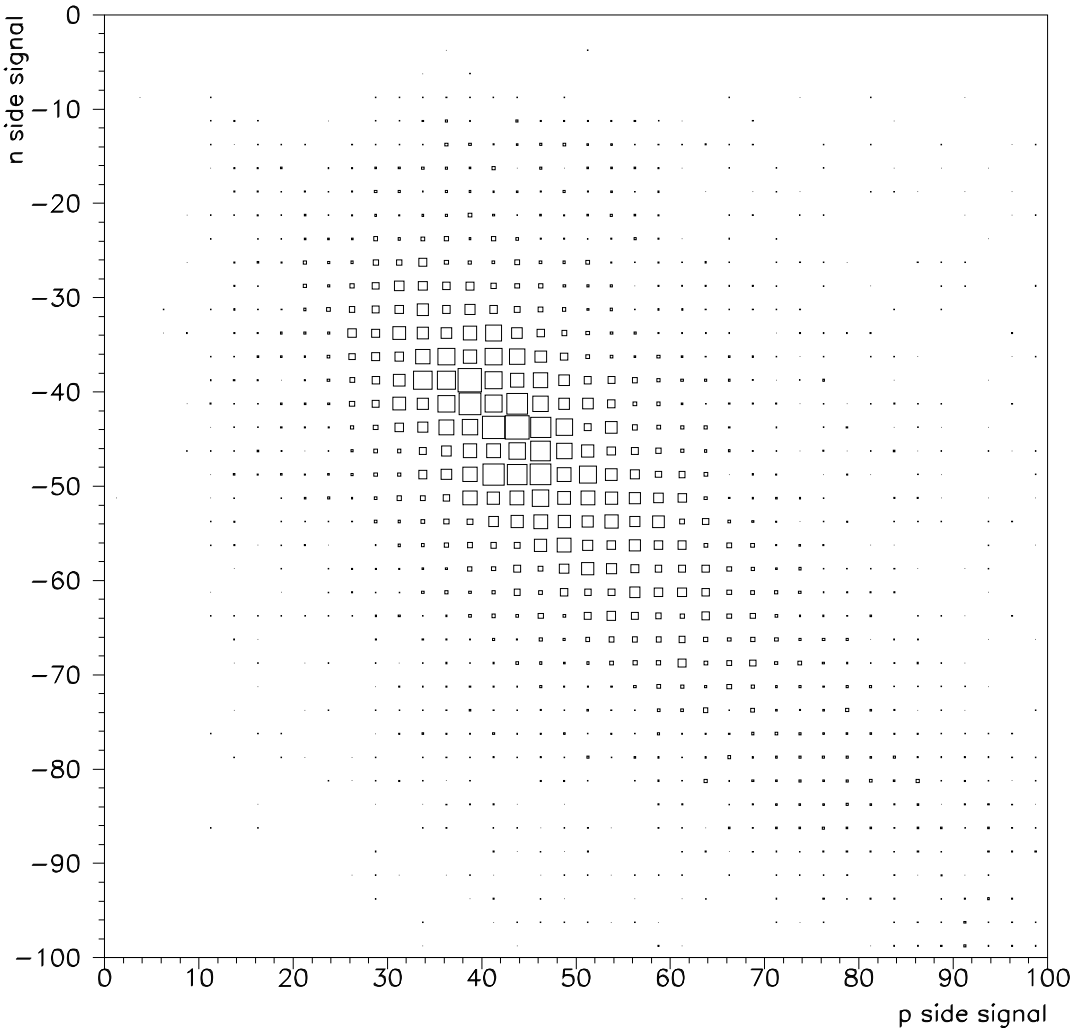

Figure 12: Landau correlation between p- and n-sides for the Outer layer.

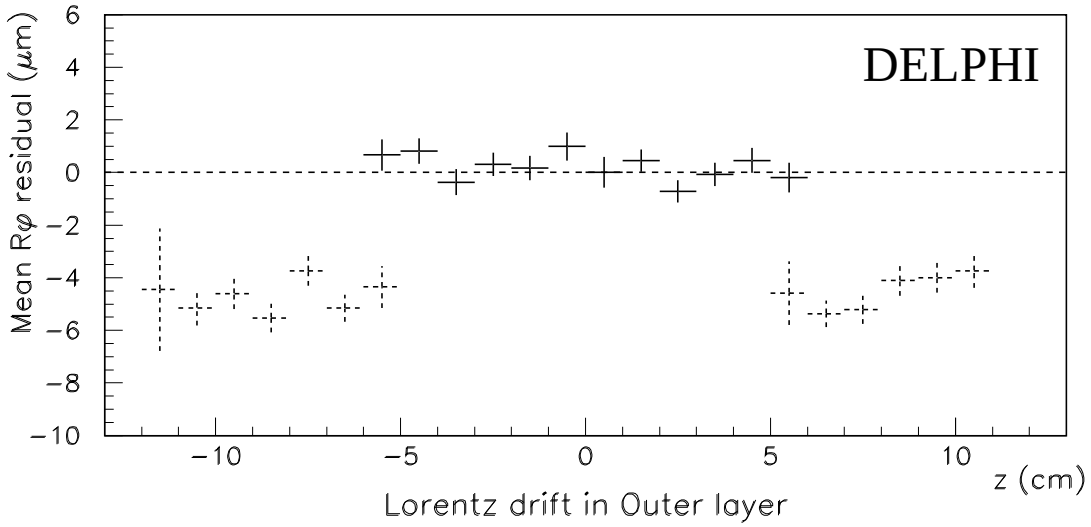

Figure 13: The mean residual in $R\phi$ for 3-hit tracks as a function of z at the Outer layer. Due to the flipped module design the E-field direction changes sign at around abs(z)=6cm, while for both Inner and Closer layers the field remains in the same direction in the polar angle interval covered by the Outer layer.

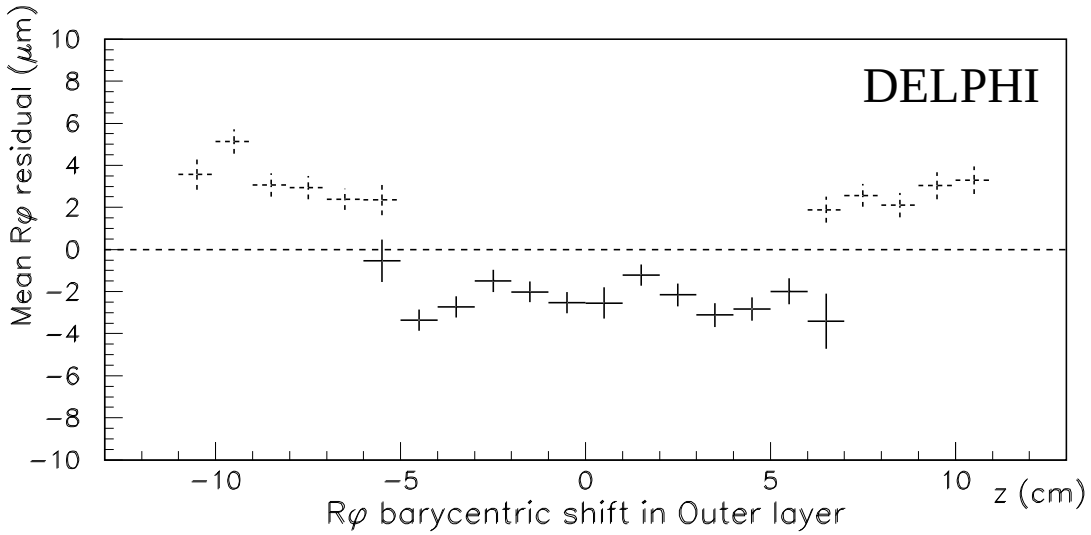

Figure 14: The mean residual in $R\phi$ for overlap tracks as a function of z at the Outer layer. Adjacent detectors have a relative angle of 15^o. Hence a radial displacement δr will appear as a shift of close to δr/4 in the $R\phi$ residual. Due to the flipped module design a barycentric shift appears as a discontinuity at abs(z)=6cm.

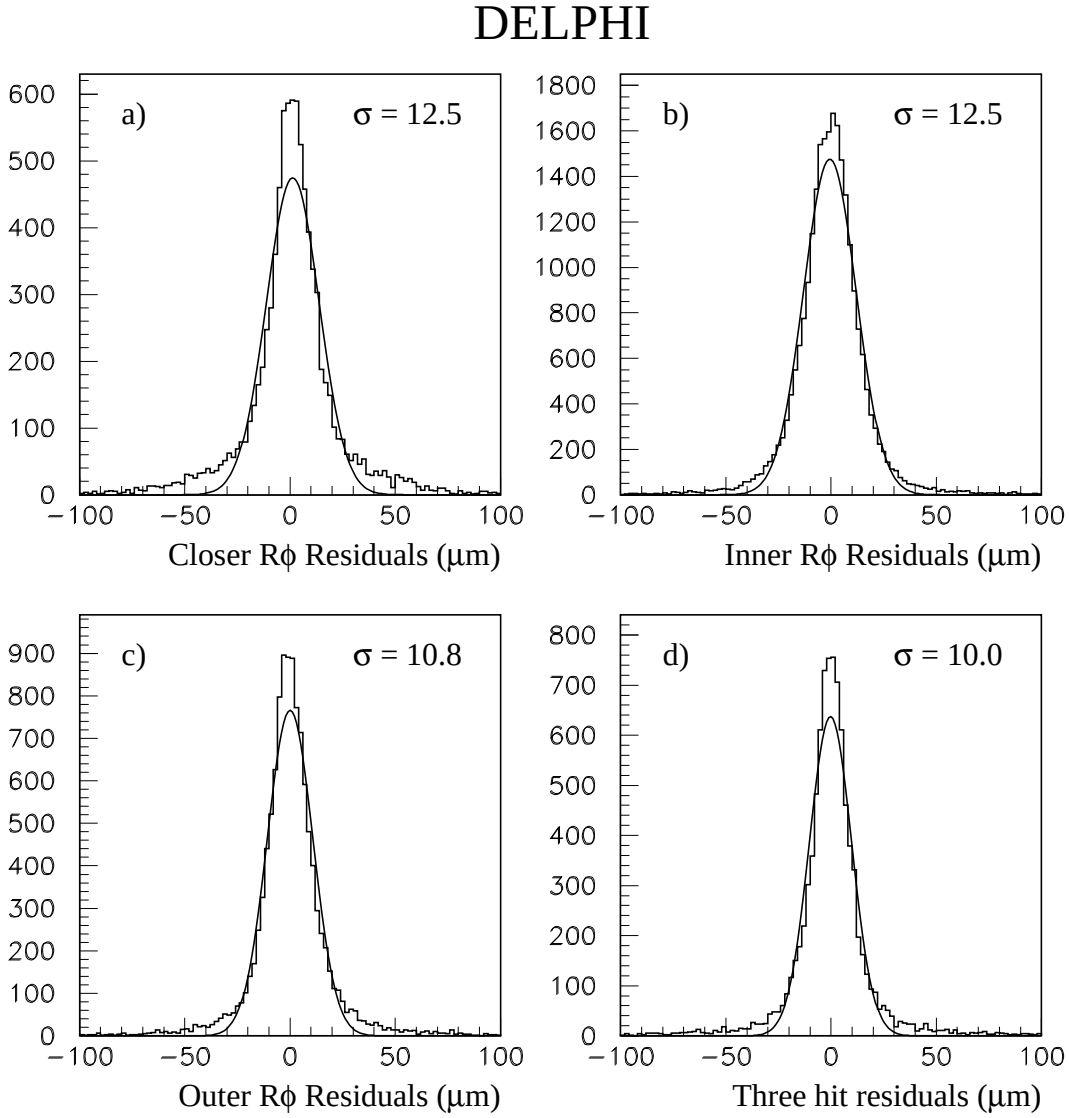

Figure 15: $R\phi$ residual distributions for a) Closer overlap tracks, b) Inner overlap tracks and c) Outer overlaps tracks. The width of each distribution has to be divided by $\sqrt{2}$ to exhibit the single hit precision for that layer of the vertex detector. Also shown are d) the Inner layer residuals for tracks with hits in all layers. Here the width has to be divided by $\sqrt{1.5}$ to obtain the silicon precision, assuming that it is the same in each of the three layers.

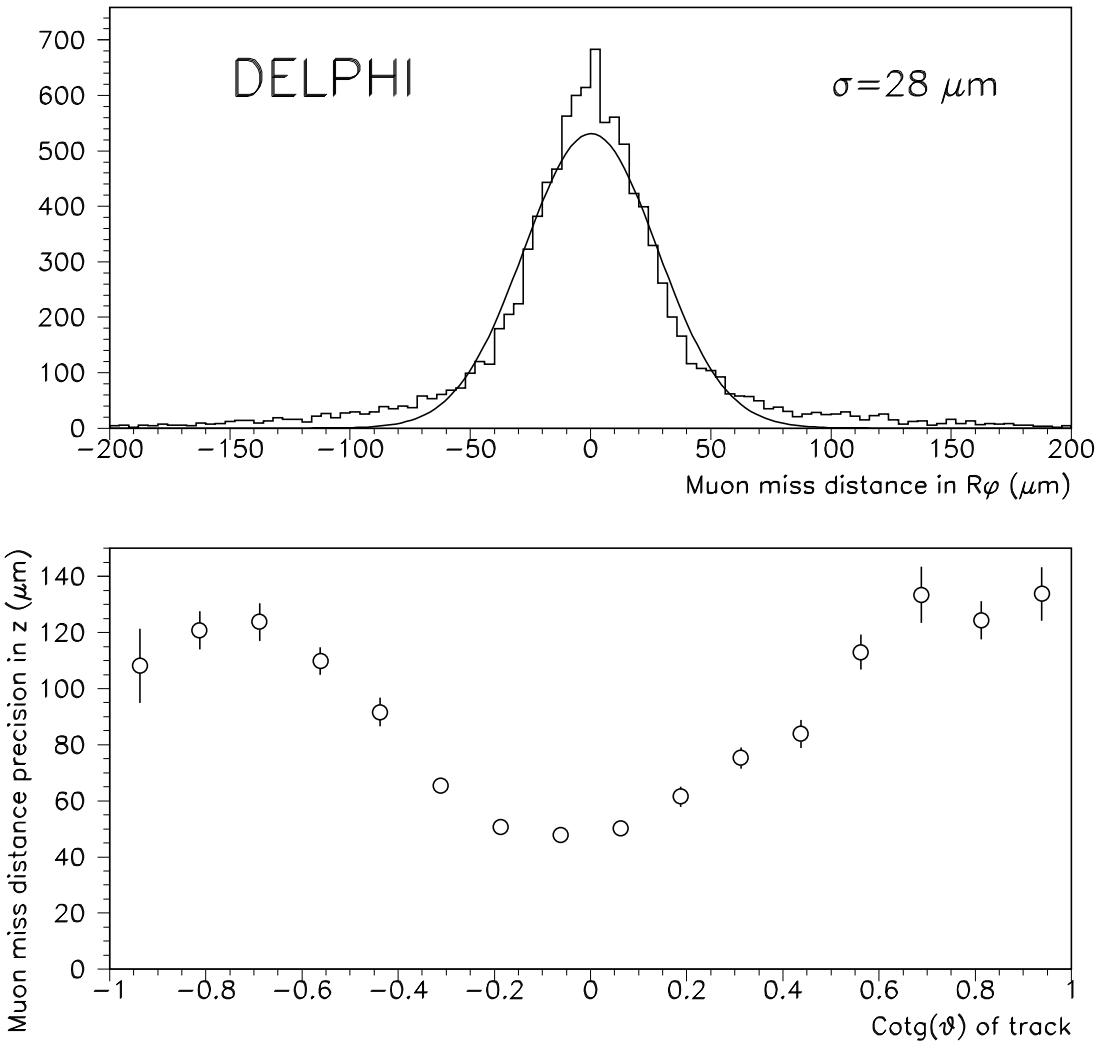

Figure 16: a) Miss distance between the two muons in $Z^0 \to \mu^+\mu^-$ in $R\phi$ plane; b) Miss distance precision between the two muons in $Z^0 \to \mu^+\mu^-$ in Rz plane as a function of the track polar angle.

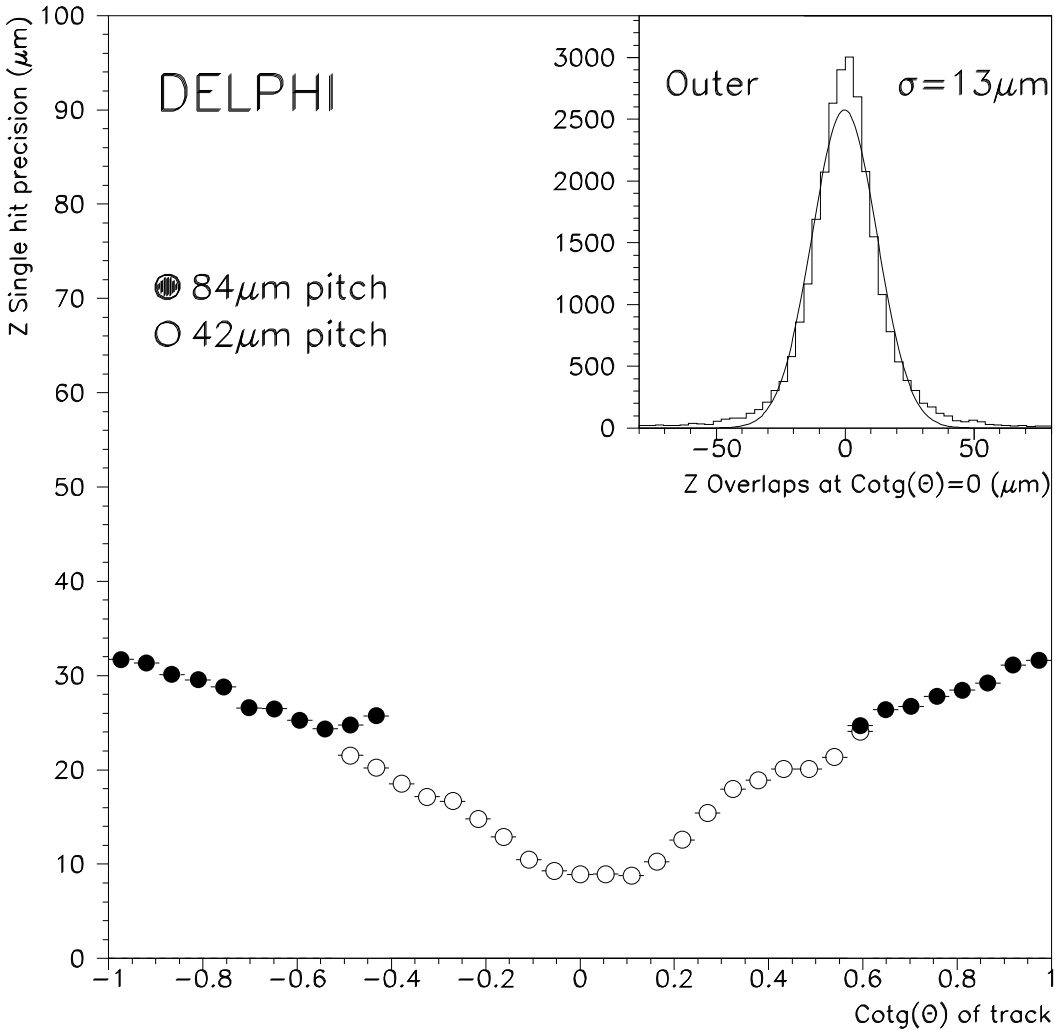

Figure 17: Outer layer z hit precision as a function of the track incident angle. The closed circles represent the region where the pitch was doubled. In the inset, z hit residuals for perpendicular particles. The width of the distribution has to be divided by $\sqrt{2}$ to exhibit the single hit precision for that layer of the vertex detector.

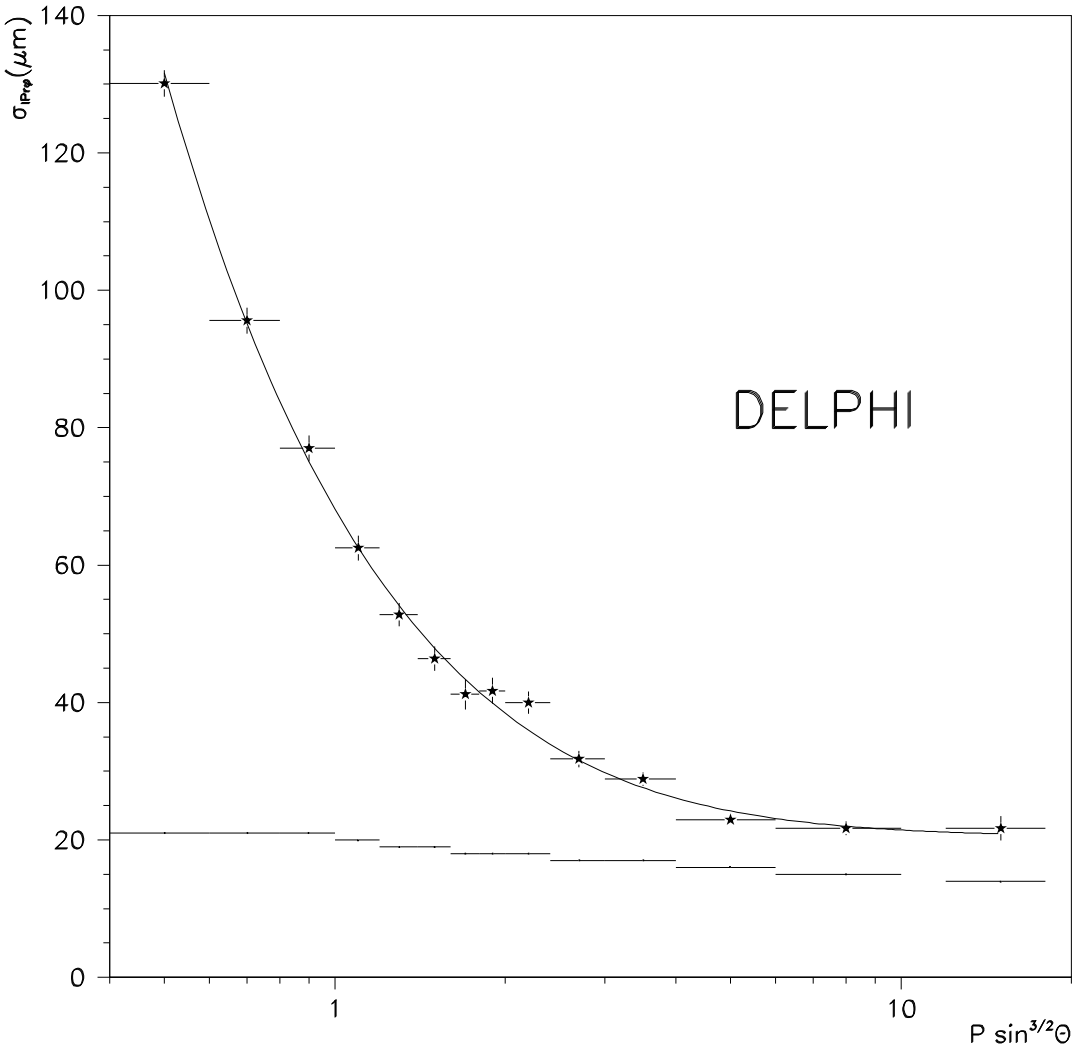

Figure 18: $R\phi$ impact parameter uncertainty measured as a function of $P\sin^{3/2}\theta$. The vertex position uncertainty, shown by the bottom curve, was quadratically subtracted. The full line is a fit to $65/p\sin^{3/2}\theta \oplus 20$

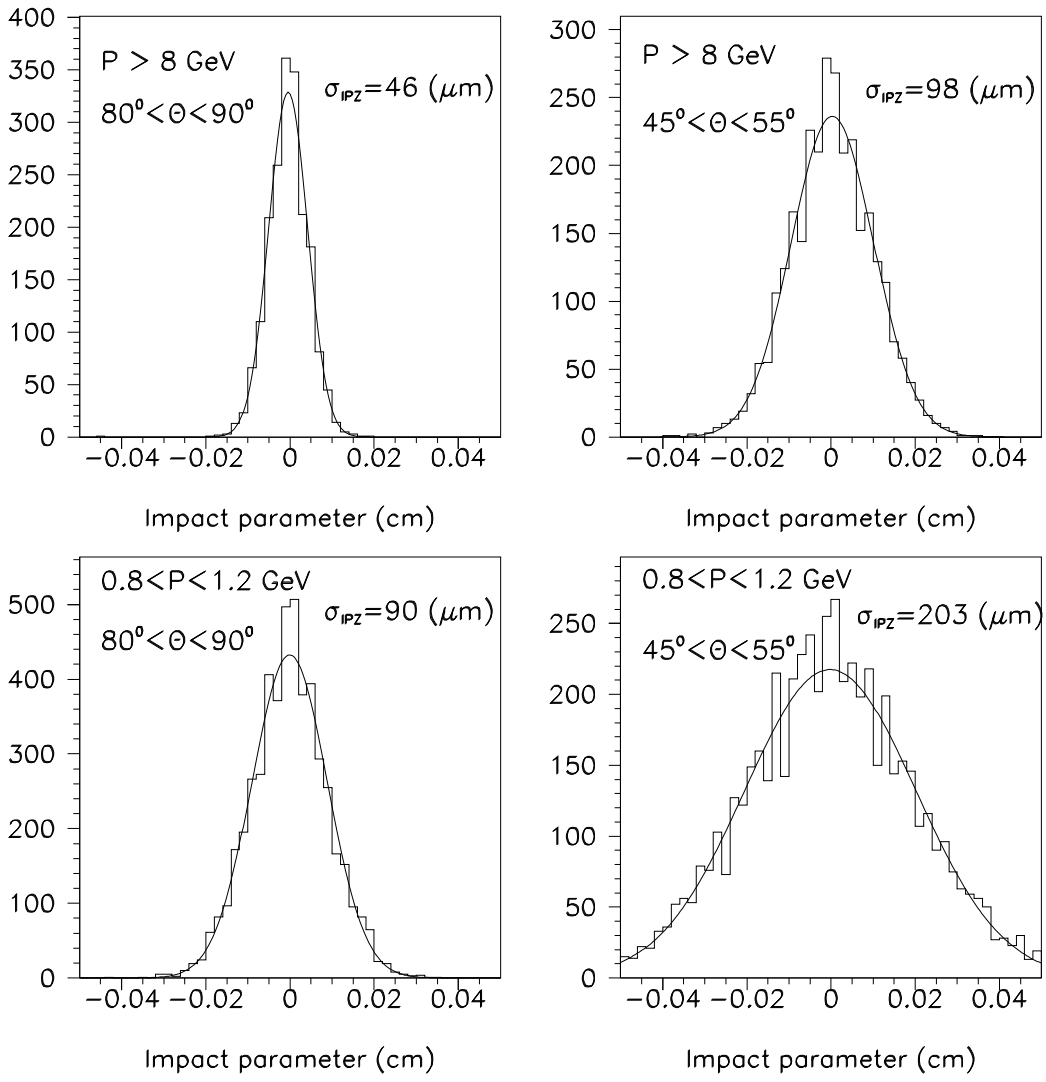

Figure 19: Impact parameter in Rz plane on real data for two different angular ranges and two momentum ranges. The vertex reconstruction uncertainty was not subtracted.

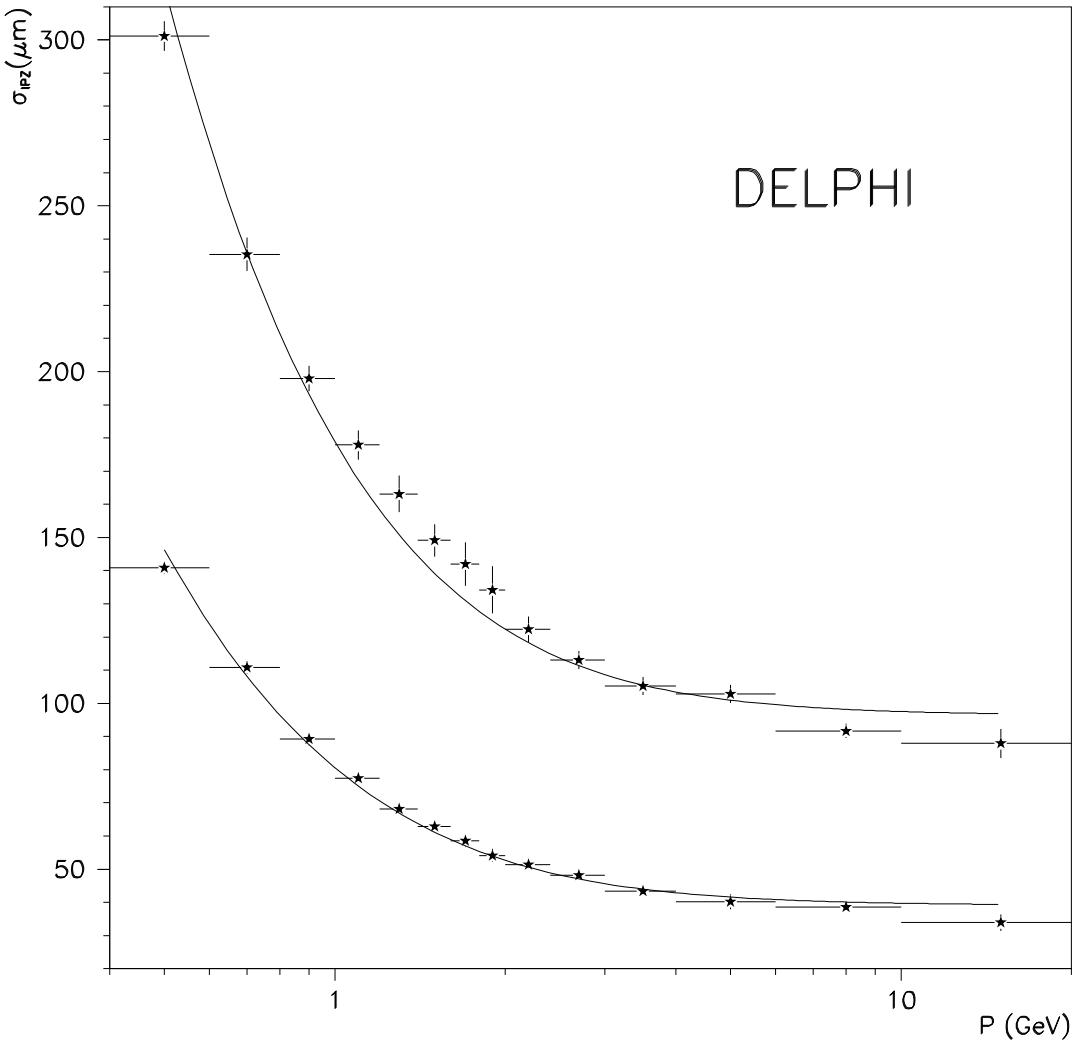

Figure 20: Impact parameter uncertainty in Rz plane, measured as a function of the particle momentum. The two curves correspond to tracks with $80^0 < \theta < 90^0$ and with $45^0 < \theta < 55^0$, respectively. The contribution from the vertex position reconstruction uncertainty was quadratically subtracted. The full lines are a fit to $71/P \oplus 39$ and $151/P \oplus 96$ respectively.

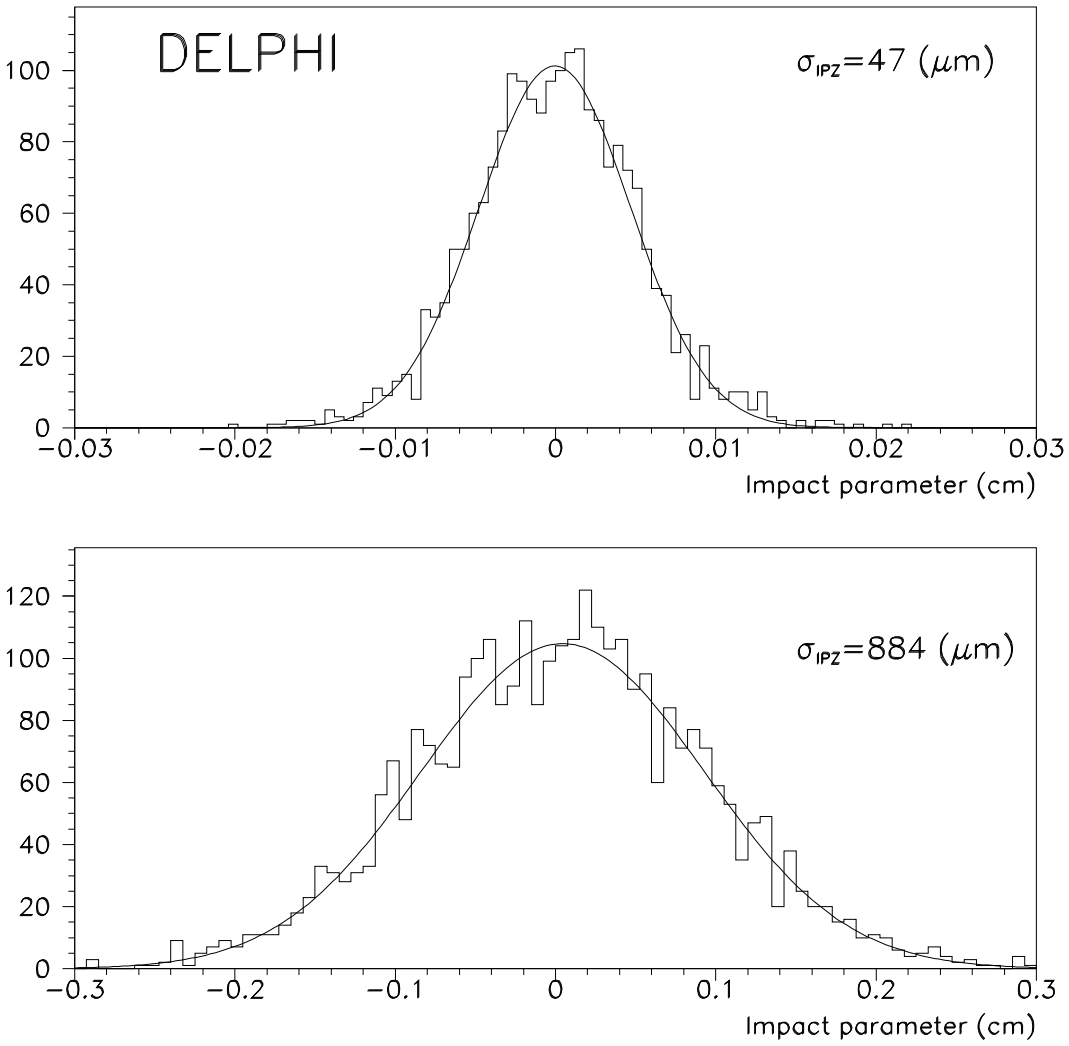

Figure 21: Impact parameter in Rz plane for P >6 GeV/c tracks ($70^0 < \theta < 90^0$) using Microvertex detector z coordinate (upper plot) and taking it out of the fit (lower plot).